minerals

MDPI

Article

The Mineral Composition and Grain Distribution of *Difflugia* Testate Amoebae: Through SEM-BEX Mapping and Software-Based Mineral Identification

Jim Buckman [1,*] and Vladimir Krivtsov [2,3]

[1] Institute of GeoEnergy Engineering, Heriot-Watt University, Riccarton, Edinburgh EH14 4AS, Scotland, UK
[2] Royal Botanic Garden Edinburgh, Edinburgh EH3 5LP, Scotland, UK; vkrivtso@exseed.ed.ac.uk
[3] 812 Livingstone Tower, Department of Mathematics and Statistics, University of Strathclyde, 26 Richmond Street, Glasgow G1 1XH, Scotland, UK
* Correspondence: j.buckman@hw.ac.uk

Abstract: We tested a scanning electron microscope equipped with the newly developed Unity-BEX detector (SEM-BEX) system to study thirty-nine samples of the testate amoeba *Difflugia*. This produces fast single-scan backscattered (BSE) and combined elemental X-ray maps of selected areas, resulting in high-resolution data-rich composite colour X-ray and combined BSE maps. Using a suitably user-defined elemental X-ray colour palette, minerals such as orthoclase, albite, quartz and mica were highlighted in blue, purple, magenta and green, respectively. Imaging was faster than comparable standard energy dispersive X-ray (EDX) analysis, of high quality, and did not suffer from problems associated with the analysis of rough surfaces by EDX, such as shadowing effects or working distance versus X-ray yield artifacts. In addition, we utilised the AZtecMatch v.6.1 software package to test its utility in identifying the mineral phases present on the *Difflugia* tests. Significantly, it was able to identify many minerals present but would require some further development due to the small size/thinness of many of the minerals analysed. The latter would also be further improved by the development of a bespoke mineral library based on actual collected X-ray data rather than based simply on stoichiometry. The investigation illustrates that in the case of the current material, minerals are preferentially selected and arranged on the test based upon their mineralogy and size, and likely upon inherent properties such as structural strength/flexibility and specific gravity. As with previous studies, mineral usage is ultimately controlled by source availability and therefore may be of limited taxonomic significance, although of value in areas such as palaeoenvironmental reconstruction.

Keywords: Unity-BEX; testate amoebae; mineralogy; grain distribution; elemental mapping

Academic Editor: Alain Chauvet

Received: 21 November 2024
Revised: 16 December 2024
Accepted: 22 December 2024
Published: 24 December 2024

Citation: Buckman, J.; Krivtsov, V. The Mineral Composition and Grain Distribution of *Difflugia* Testate Amoebae: Through SEM-BEX Mapping and Software-Based Mineral Identification. *Minerals* **2025**, *15*, 1. https://doi.org/10.3390/min15010001

1. Introduction

Testate amoebae are ubiquitous in many freshwater and terrestrial environments, yet less well known in comparison to other protists, such as foraminifera, diatoms and radiolaria. They construct their tests in one of three ways: (1) formation of a purely organic test, (2) internal production of silicious or calcitic plates (idiosomes) or (3) collection and reuse of particulates from the environment (xenosomes). The latter may be inorganic detrital mineral particles or biogenic (e.g., diatoms, algal cysts, reworked idiosomes from other testate amoebae). Here we look at xenosome-bearing examples of the testate amoebae *Difflugia*, which utilise particulate material (primarily detrital inorganic) collected from an isolated freshwater pond system (see [1]). Xenosomes used are often quartz grains but

can be more variable in nature, controlled by selection preferences and the types and sizes of grains that are available [2,3]. Previous papers have used X-ray tomography (XRT) to characterise the 3D morphology of grains and their spatial distribution within the test of xenosome-bearing testate amoebae (see [3]). ESEM-EDX has also been used to characterise the elemental composition of such grains in polished thin sections [3], as well as illustration from rough surfaces [1,2]. The latter can suffer from shadowing effects due to the surface relief between particles and the positioning of the EDX detector. Additionally, neither XRT nor SEM-EDX analysis directly identify grain mineralogy. Here we use SEM equipped with a Unity-BEX combined backscattered and characteristic X-ray detector to produce fast elemental composition colour maps across the whole exposed surface of thirty-nine samples of *Difflugia* with a simple vase-like morphology that is typical of the genus. We also use AZtecMatch to test the possibility of formally identifying the mineral phases present across six randomly selected examples of the examined samples, as well as identifying additional mineral phases amongst all thirty-nine samples studied. In addition, we examine the distribution of particle size, shape and composition across the surface of the test from the aperture and fundus ends of the test.

2. Material and Methods

Thirty-nine specimens of *Difflugia* examined from a community of testate amoebae, collected in July 2018 from an unnamed pond adjacent to the Gore Water, Gore Glen Woodland Park, Gorebridge, Scotland (Figure 1).

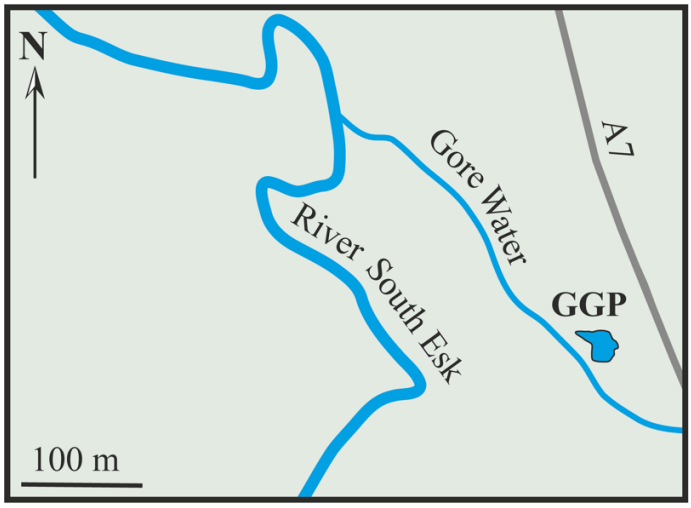

Figure 1. Locality map of Gore Glen Woodland Park, between the Gore Water and A7. Specimens collected from the Gore Glen Pond (GGP). See Google Maps for further locality details.

Samples were examined in an uncleaned state, with no form of sample preparation other than direct filtering on to polycarbonate filter paper with 1 µm pores. The filter was lightly gold-coated using an Emitech K550 sputter coater. Imaging utilised a Quanta 650 FEG scanning electron microscope (SEM), operated in high vacuum mode at 15–20 kV, spot size 5 and aperture setting no. 1. This was set to optimise X-ray flux over image quality. Settings produced a useable X-ray output count rate in the order of 900,000 cps. Elemental maps were constructed using an X-Max^N 150 mm EDX detector in conjunction with a Unity-BEX detector system (Oxford Instruments). Data were collected in a single scan of combined BSE and X-ray map, with thirty-three samples having a scan time of 65 µs (~5 min per image/map) and six at 400 µs (~20 min) and an image size of 2048 × 1465 pixels. All elements were collected for each pixel per map, with Si, Al, K, Na, Ca, Mg, Fe, Ti and S selected and displayed to show the occurrence and distribution of

silicates (quartz, feldspars, micas, clays) and other mineral phases (carbonates, sulphides, heavy minerals). A colour scheme was developed to best illustrate mineral distribution using AZtec Unity-BEX (Table 1).

Table 1. Colour settings used in AZtec BEX, overview maps (Figures 2 and 3, File S1 in Supplementary Material).

Element	Colour	R, G, B	Hue
Si	Magenta	255, 0, 255	300
Al	Green	84, 255, 0	100
K	Teal	0, 255, 255	180
Na	Dark blue	0, 42, 255	230
Ca	Red	255, 0, 42	350
Mg	Orange	255, 212, 0	50
Fe	Yellow	255, 255, 0	60
Ti	Yellow 2	255, 191, 0	45
S	Yellow 3	233, 255, 0	65

In addition, for the six main samples studied, fifty representative grains were selected from each specimen (300 in total) and characterised in terms of their mineral composition and spatial distribution. Minerals were identified using AZtecMatch with the addition, where necessary, of manual interpretation using elemental composition (from the X-Max^N 150 mm and Unity-BEX detectors) and morphological features such as flatness, blocky form, sphericity, etc. In addition, the majority of particles on the six samples were measured in terms of their maximum length, with each specimen divided into front half (nearest aperture) and back half (nearest the fundus).

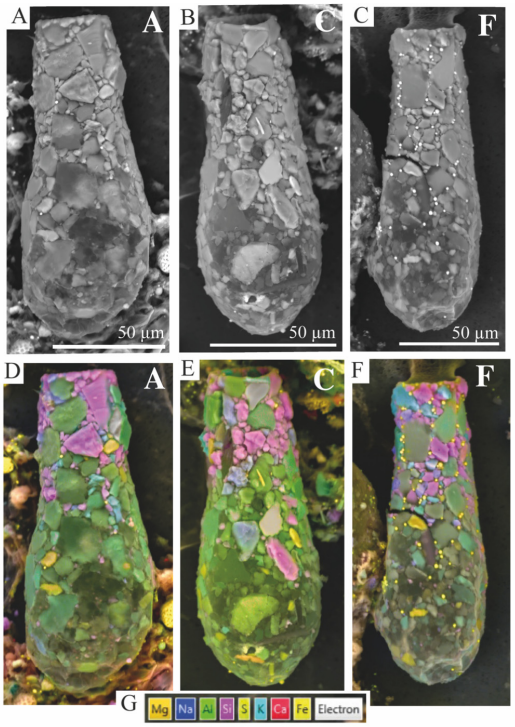

Figure 2. *Difflugia* sp., morphotype-A, cf *Cylindrifflugia lanceolata* (Penard, 1890) n. comb. Gonzalez-Miguens et al., 2022. (**A**–**C**) Backscattered (BSE) images of three selected examples. (**D**–**F**) Corresponding BSE and (**G**) elemental colour overlay maps for Mg, Na, Al, Si, S, K, Ca and Fe. White letters refer to specimen ID.

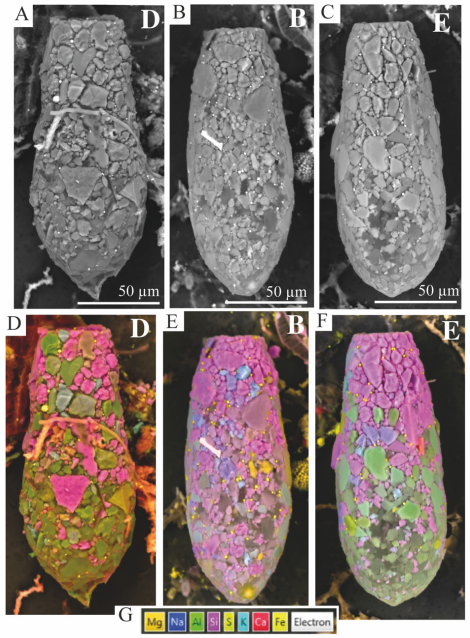

Figure 3. *Difflugia* sp., morphotype-B, cf *D. linearis* Penard, 1958. (**A**–**C**) Backscattered (BSE) images of three selected examples. (**D**–**F**) Corresponding BSE and (**G**) elemental colour overlay maps for Mg, Na, Al, Si, S, K, Ca and Fe. White letters refer to specimen ID.

3. Results

All samples were successfully imaged and mapped in terms of elemental and mineral distribution. Results for BSE images and combined overlaid elemental maps are shown in Figures 2 and 3 (see also File S1 in Supplementary Material).

3.1. Taxonomy

Siemensma [4] lists more than 170 species of described *Difflugia* species (including eight transferred to *Cylindrifflugia*). Due to the taxonomic complexity of such material, they are here only identified as *Difflugia* sp., morphotype-A and morphotype-B. Measured parameters are illustrated in Figure 4.

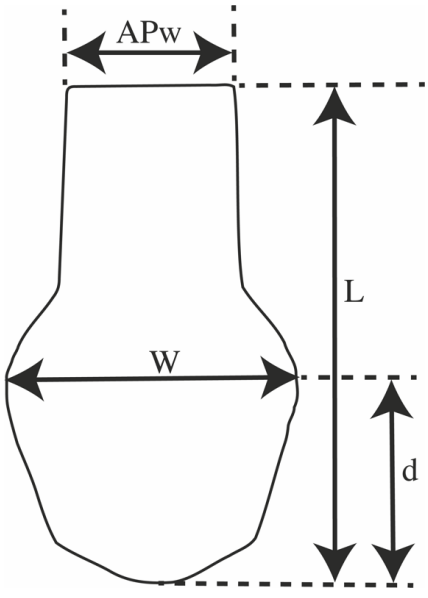

Figure 4. Parameters measured in the present study. APw = aperture width, W = test width, L = test length, d = distance of widest part of test from fundus.

Difflugia sp., morphotype-A c.f. *Cylindrifflugia lanceolata* (Penard, 1890), Gozález-Miguéns et al., 2022, *Difflugia oblonga* Ehrenburgh 1838. Figure 2, File S1 in Supplementary Material.

Samples: Seventeen examples (B, D, D1–2, D6–7, D10, D13–15, D19–21, D24, D30, D33, E)

Description: Relatively simple ovoid (acuminate) test, tapering towards the aperture. Length 101–172 µm (average 140 µm), width 42–74 µm (average 61 µm) (Figure 5, Table 2). Widest part 1/3rd–1/4th the length from the fundus. Aperture 25–43 µm wide (average 32 µm). Surface typically rough towards the aperture end, covered in blocky or granular framework silicate minerals, and smoother towards the fundus, where it comprises sheet-silicates, or is dominated by blocky minerals throughout, giving an overall rougher surface (Figure 2, File S1 in Supplementary Material).

Table 2. Physical attributes, for morphotype-A and -B.

Morphotype		Length	Width	Aperture	d/L
A	Average	140	61	32	0.3
	Min.	101	42	25	0.3
	Max.	172	74	43	0.4
	SD	19	8	5	0.04
	Covariance	7	8	7	9
	n=	17	17	17	17
B	Average	134	55	32	0.3
	Min.	103	47	22	0.2
	Max.	165	63	44	0.4
	SD	14	5	4	0.05
	Covariance	9	12	8	7
	n=	22	22	22	22

d/L = distance of widest part of test from posterior/length of test.

Difflugia sp., morphotype-B c.f. *Difflugia linearis* (Penard, 1890) Gauthier-Lièvre and Thomas, 1958. Figure 3, File S1 in Supplementary Material.

Samples: twenty-two examples (A, C, D2–5, D8–9, D11–12, D16–18, D22–23, D25–29, D31–32, F).

Description: Pyriform in shape, 103–165 µm (average 134 µm), width 47–63 µm (average 55 µm) (Figure 5, Table 2). Widest part 1/2th–1/4th the length from the fundus. Aperture width 22–44 µm (average 32 µm). Typically, rough surface towards aperture end, with granular/blocky grains, while smoother towards the fundus, where covered by thin sheet-silicates such as muscovite (Figure 3, File S1 in Supplementary Material).

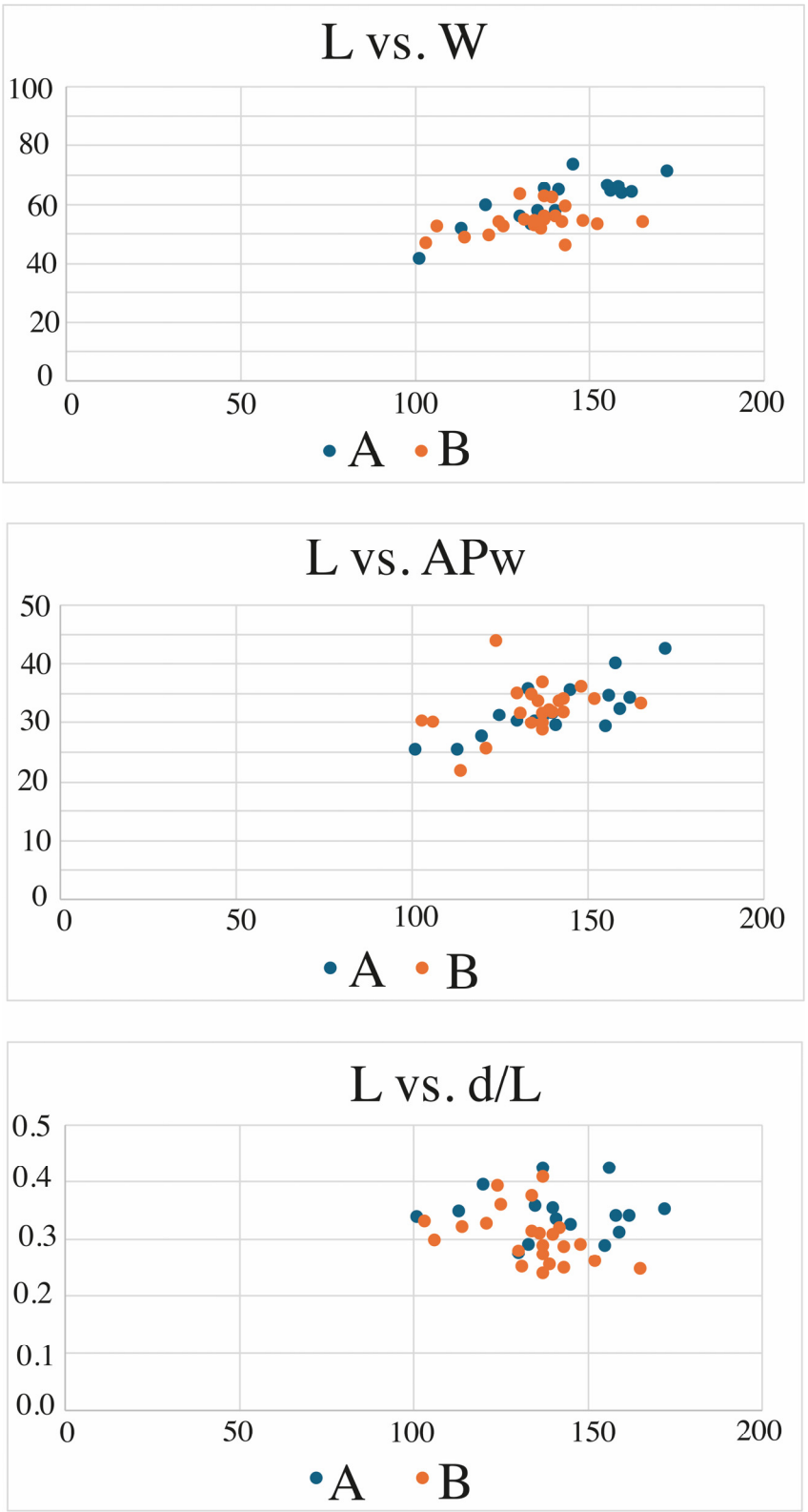

Figure 5. Parameter graphs in microns for length (L) versus width (W), length versus aperture width (APw), and length versus the ratio of distance of widest part from fundus/length (d/L). A = *Difflugia* sp. morphology-A, B = *Difflugia* sp. morphology-B.

3.2. Mineralogy

Colour overlay maps derived using AZtec Unity-BEX clearly indicate the occurrence of a range of distinct mineral phases, coloured magenta, blue, purple, green, orange and

yellow (Figures 2 and 3, File S1 in Supplementary Material). A combination of data from these maps and analysis of selected grains by AZtecMatch indicates that the main mineral phases are quartz, feldspars (alkali/K-feldspars, plagioclase feldspars), micas (muscovite and biotite), kaolin and pyrite, with smaller amounts of minor phases such as calcite and hornblende, as well as the heavy minerals apatite, rutile, ilmenite, garnet and zircon (Table 3). In addition, biogenic silica, lithic fragments and patches of biofilm also occur.

Table 3. Numbers of individual mineral phases identified with AZtecMatch.

Group	Mineral	A	B	C	D	E	F	D1-D33	Total
Framework silicates	Quartz	11	13	9	10	9	7		59
	Orthoclase	1	7	3	8	5	5		29
	Anorthoclase	2	3		2		1		8
	Albite	2	7	9	7	7	4		36
	Andesine			1					1
	Oligoclase	1							1
	Ca-plagioclase *							1	1
	Feldspar						1		1
Sheet silicates	Kaolin	13	5	8	4	4	9		43
	Muscovite	15	7	13	11	15	16		77
Mg-Fe silicates	Biotite	1	2	1				3	7
	Garnet					2		13	15
	Hornblende		1	2				4	7
Heavy minerals	Pyrite	2	3	2	3	5	3		18
	Rutile			2					2
	Zircon		1						1
	Ilmenite							8	8
	Apatite							8	8
Carbonates	Calcite							3	3
Fe oxides	Goethite							3	3
									328

* Bytownite/labradorite/anorthite.

3.2.1. Quartz

Grains of quartz occur as magenta-coloured areas in composite maps (Figures 2 and 3, File S1 in Supplementary Material). Grain sizes range from around 2 to 25 or 30 μm and typically appear granular in form (File S1 in Supplementary Material). Quartz occurs throughout the test but is more abundant towards the aperture end of the test, where all larger quartz grains are found (Figures 2 and 3, File S1 in Supplementary Material). In several cases, smaller equant grains of quartz occur around the aperture (File S1 in Supplementary Material, specimen A and E).

3.2.2. Feldspar

AZtecMatch identified a number of feldspars as candidate particles, with plagioclase feldspar (albite, oligoclase, andesine) and alkali/K-feldspar (anorthoclase, sanidine and orthoclase/microcline). In general, using the chosen elemental colouring scheme (Table 1),

it was possible to differentiate between plagioclases (albite, oligoclase, andesine), which are purple, and K-feldspar (orthoclase) in blue. Anorthoclase was identified, although occurring with either a blue (n = 3), purple (n = 4) or in one case no colour on composite-coloured elemental maps. In addition, one orange-coloured particle was assigned to andesine and one (colourless) particle to oligoclase, while one sample (purple) could not be differentiated between anorthoclase (alkali feldspar) and andesine (plagioclase feldspar) and is here assigned as feldspar only. In addition, one grain of a more calcic plagioclase feldspar was identified as bytownite, labradorite or anorthite (D19).

The K-feldspars (blue) contained 7–18 atomic% K (average 13), 0–10 atomic% Na (average 1) and 0–2 atomic% Ca (average 0). Na-rich plagioclase feldspars (purple) comprised 0–5 atomic% K (average 1), 8–19 atomic% Na (average 15) and 0–3 atomic% Ca (average 0).

As with quartz, larger feldspars are typically concentrated within the half of the test closest to the aperture. Smaller feldspar grains can be associated with quartz around the aperture, and grains around 2 µm are found sporadically across the test filling gaps between the larger grains.

All feldspars are typically blocky in appearance and range from 2 to 59 µm in size. A few feldspar grains are more elongated in form and typically orientated approximately parallel to the test's long axis (Table 4, File S1 in Supplementary Material: D7, D9, D32).

Table 4. Samples with conspicuously larger singular grains within their test structure.

Specimen	Particle L × W	Aperture	Composition	Orientation
D4	24 × 23	25	Musc/Kaolin	N/A
D7	54 × 9	29	K-spar	Parallel test
D9	32 × 8	27	K-spar	Parallel test
D11	21 × 17	30	Kaolin	N/A
D12	21 × 15	15	Muscovite	N/A
D18	35 × 16	35	Muscovite	Parallel test
D26	40 × 30	28	K-spar	N/A
D32	59 × 17	34	K-spar	Parallel test

3.2.3. Muscovite/Kaolin

Both appear as green on the composite X-ray maps (Figures 2 and 3, File S1 in Supplementary Materials). AZtecMatch identified nacrite/dickite/halloysite/kaolinite (kaolin) and muscovite as present. Muscovite and kaolin have a thin sheet-like appearance, sometimes hexagonal in shape, forming surfaces where grains interlock or slightly overlap. Some kaolin from closer to the aperture are blockier in appearance. Muscovite and kaolin range in size from around several microns up to 35 µm (Table 4). Both occur more dominantly in the half of the test closest to the fundus, which is particularly obvious in *Difflugia* sp. morphotype-B (see File S1 in Supplementary Material).

3.2.4. Pyrite

Pyrite appears as yellow on composite X-ray maps (Figures 2 and 3) and occurs as small (under 2 µm) single multi-faceted crystals that are typically embedded within the organic cement that occurs between major silicate grains (Figure 6). The surface of pyrite grains has a mottled texture (Figure 6B). Pyrite was noted to occur to a variable degree, from not present, to present to a minor degree, to over 50 observed particles in a single test (one side only) (Figures 2E and 3F). It should also be noted that pyrite can occur in highly dense masses (illustrated in [1]).

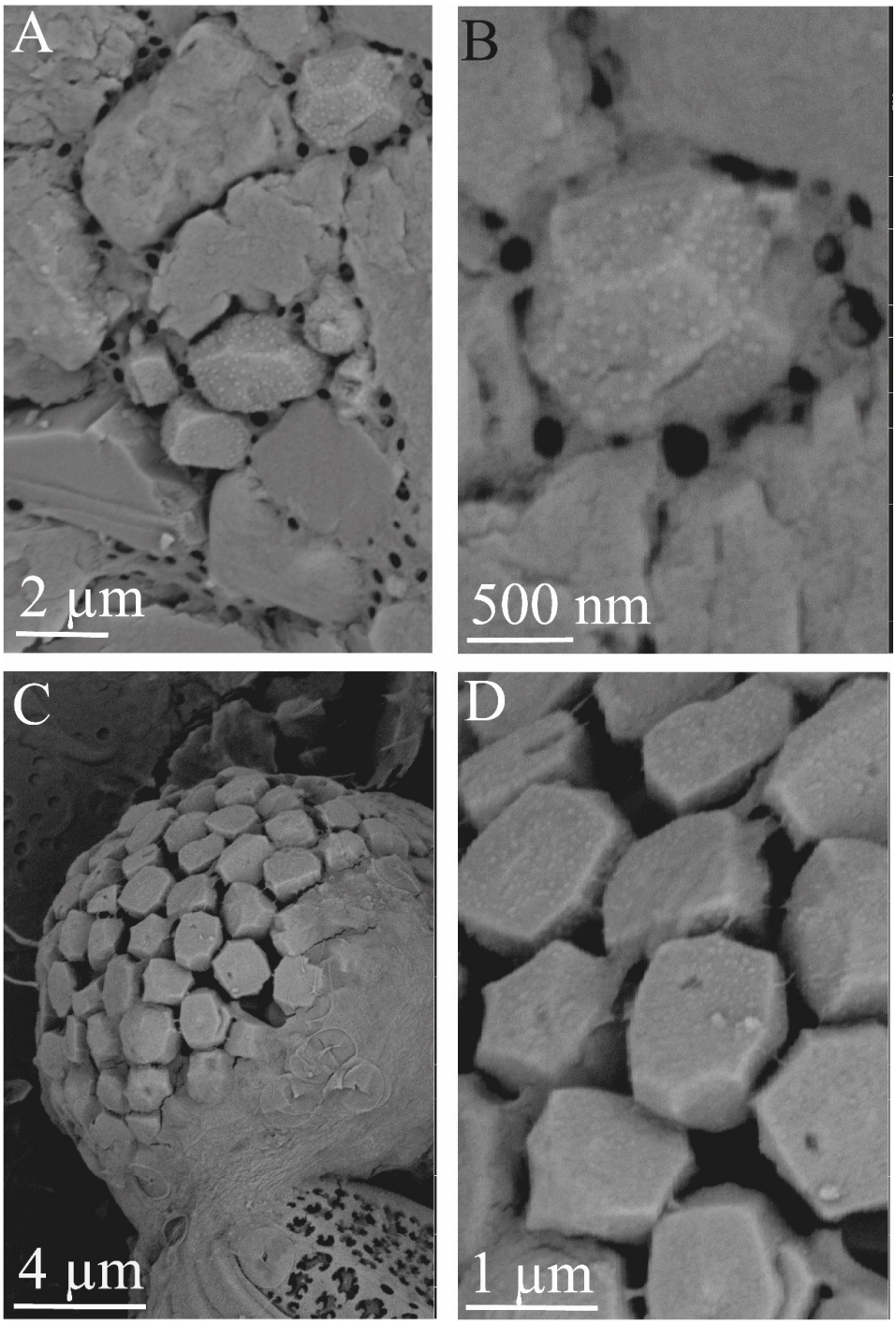

Figure 6. (**A**,**B**) Details of pyrite crystals utilised within *Difflugia*. (**C**,**D**) Pyrite framboid developed within chrysophacean cyst cell.

3.2.5. Fe Oxide

Rare, with three examples identified as goethite (specimens D5, D7, D31), having a yellow colouration in X-ray overlay maps. Shape angular and between 3 and 10 µm in size.

3.2.6. Calcite

Calcite was noted in two samples (D22, 31), having an orange colour on composite maps, identified as calcite on composition and morphology, and as calcite/aragonite in AZtecMatch. Appearing with a radial acicular-like structure, with five dumbbell-shaped examples (Figure 7C). Particles are under 5 µm in length.

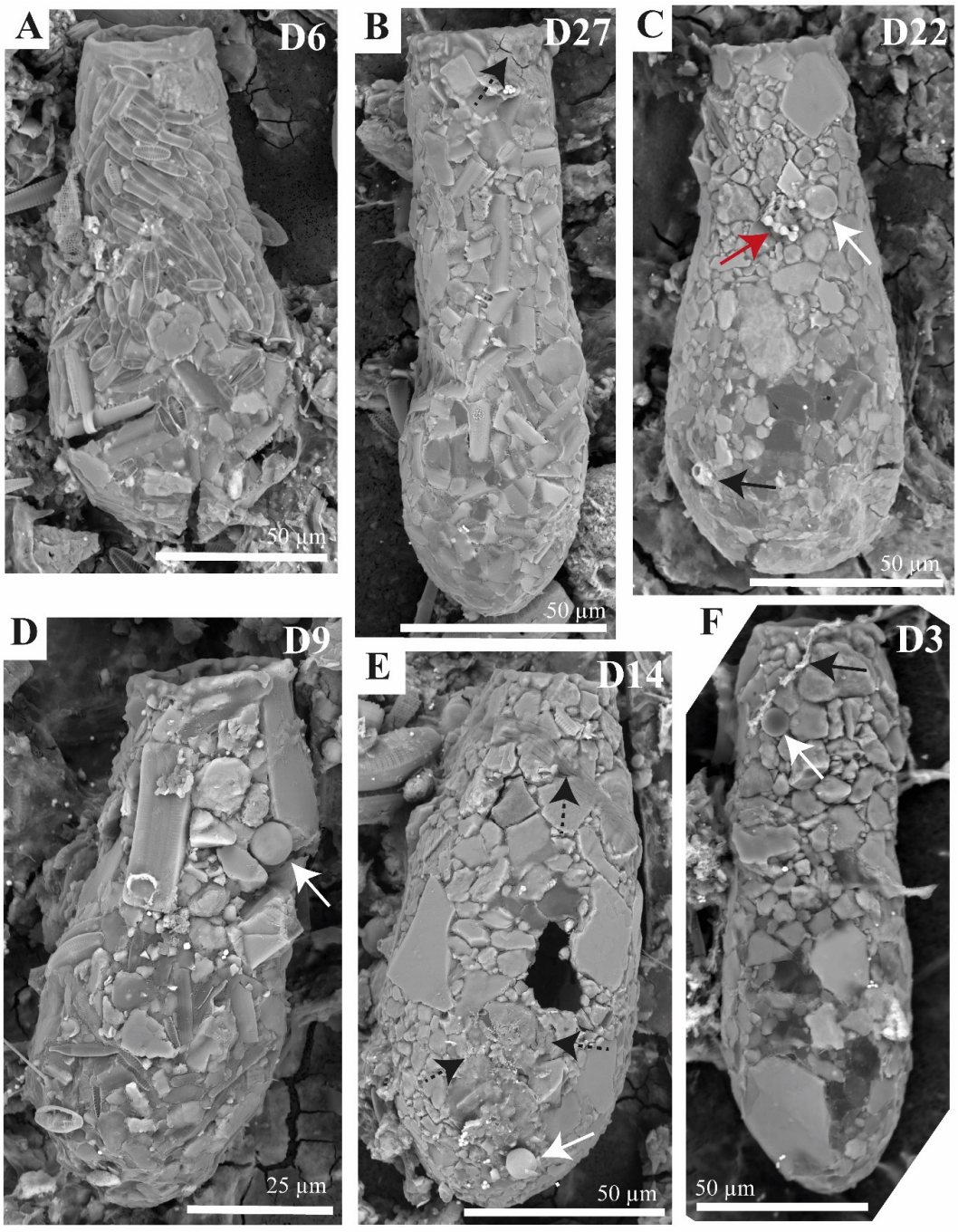

Figure 7. BSE images of *Difflugia* illustrating the use and occurrence of biogenic material associated with the tests. (**A**) Test covered by intact diatom frustules. (**B**) Dominated by fragmentary diatom frustules. (**C**–**F**) Isolated siliceous algal cysts (white arrows). Note the variation in numbers of associated diatom frustules. Additionally, black solid arrow = conical-shaped and stringy Fe-Mn biofilm components. Dashed arrow = thin C-rich biofilm. Red arrow = dumbbell-shaped $CaCO_3$ precipitate. White letters refer to specimen ID.

3.2.7. Apatite

Noted in seven specimens (D13, 17, 22–23, 25, 29–30). Orange in colour, apatite inferred from the co-occurrence of Ca and P and identified by AZtecMatch. Shape angular, sometimes diamond-shaped or triangular and typically 10 to 20 µm in size.

3.2.8. Zircon

Only observed from one sample (B), as an elongated grain, approximately 15 µm in length and 3 µm wide. Appearing white (colourless) in composite maps.

3.2.9. Rutile

Rare, with two examples on one sample (Figure 3E). Yellow in colour on composite maps, identified by the co-occurrence of Ti and O and lack of Fe. Shape blade-like or sheet-like, and size 10 × 1 to 3 µm.

3.2.10. Ilmenite

At least seven samples contained Fe-Ti rich minerals in minor quantities (D8, 11–12, 15–16, 21, 33). Yellow in composite maps, identified as ilmenite in AZtecMatch. Shape angular, platey to prismatic and 10–25 µm in size.

3.2.11. Mg-Fe Minerals

A number of particles had appreciable amounts of Mg and Fe, along with Si and Al (D8–10, 13, 16, 19–21, 23, 25, 28–29), representing a contingent of ferro-magnesian minerals. These were harder to differentiate, but according to AZtecMatch were identified as mainly almandine garnets (compositionally towards pyrope, with Mg present), with biotite (D19, 20), ferrohornblende (D23), magnesiohornblende (D29) and amphibole (D29). Grains typically angular, 5 to 30 µm in size, and appearing yellowy-green in composite colour maps (Figures 2 and 3, File S1 in Supplementary Material).

3.2.12. Biogenic Silica

At least thirteen samples have incorporated diatoms within their test structure to a variable degree (D5–6, 8–9, 11–13, 17–20, 27, 33), with D6 and 27 dominated by diatoms (Figure 7A,B). In addition, four samples incorporated at least a single algal cyst (D3, 9, 14, 22) (Figure 7C–F). Biogenic silica is variable in size, with algal cysts typically under 10 µm, and diatom frustules from 5 up to 30 µm or so, dependent on diatom species. Notably tests can also utilize whole specimens of small *Trachelocorythion pulchellum* (a testate amoebae comprising siliceous idiosomes), as illustrated by Krivtsov et al. [1] from this locality.

3.2.13. Lithic Fragments

One lithic fragment (16 × 14 µm in size) observed in sample D18 (File S1 in Supplementary Material), comprising feldspars, quartz and iron-rich minerals.

3.2.14. Patchy Biofilm

Materials interpreted as having an origin as biofilm are relatively rare. Two types occur: (i) thin grain covering organic film on the top of mineral grains, with a cracked surface due to dehydration (Figure 7E) and (ii) conical-shaped structures of Fe-Mn rich biofilm, around 5–10 µm in size, with a central orifice (Figure 7C) and associated Fe-Mn biofilm strings several microns in width (Figure 7F).

3.3. Grain Size, Shape and Mineralogical Distribution

For the six examples studied in detail, grains were typically less than 10 to 15 µm, with asymmetric grain distribution, skewed towards the coarser side (Figure 8). Average grain size of selected particles between 3.7 and 8.3 µm (samples A–F), with a maximum observed size of 33.8 µm (sample D; Figure 9), minimum recorded size 441 nm. The 25%–75% quartile over the 6 samples range from 1.39 to 10.2 µm.

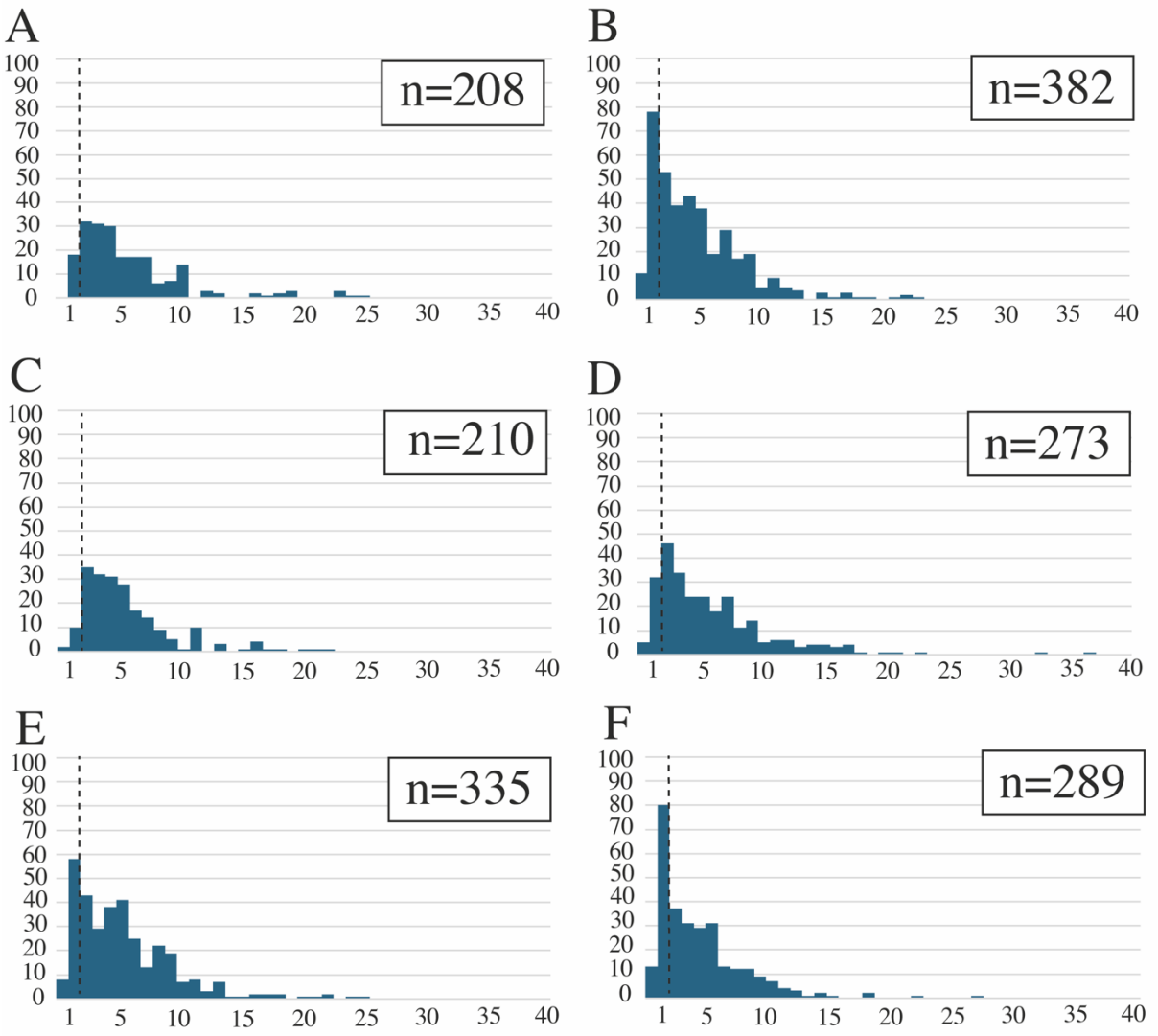

Figure 8. Grain size distribution measured from sample (**A**–**F**). Dashed line marks the boundary between clay and silt grains (2 μm). Vertical axis = number of counts, horizontal axis = grain size (μm).

For morphotype-A, the front and back halves of the test have similar metrics (B), or the front exhibits a slightly greater range in terms of the 25%–75% percentiles (D, E), and in all cases have large outliers towards the front half of the test (Figure 9). In morphotype-B, two examples have lower 25%–75% percentile ranges for the front half of the test (A, F) and one with a slightly higher 75% percentile towards the front, all three having larger outliers associated with the front half of the test (Figure 9). Therefore, although some differences are noted between the two morphotypes, no clearcut differentiation can be made. Within the additional thirty-three specimens examined occasional grains up to 54 and 59 μm in length also occur (File S1 in Supplementary Material, D7, D32; Table 4).

Many of the larger grain fraction are blockily cuboidal in form (feldspars); others are more granular (quartz), sheet-like (micas and kaolin), or occasionally the largest grains are elongated and blade-like in shape (See File S1 in Supplementary Materials for variability). The smallest particles (typically 1–2 μm) are single crystals of pyrite, which appear spherical, but form small, faceted crystals. However, the smaller fraction (<2 μm) also includes particles of quartz and feldspar. No clays (illite, smectite etc.) were observed from the clay-sized fraction.

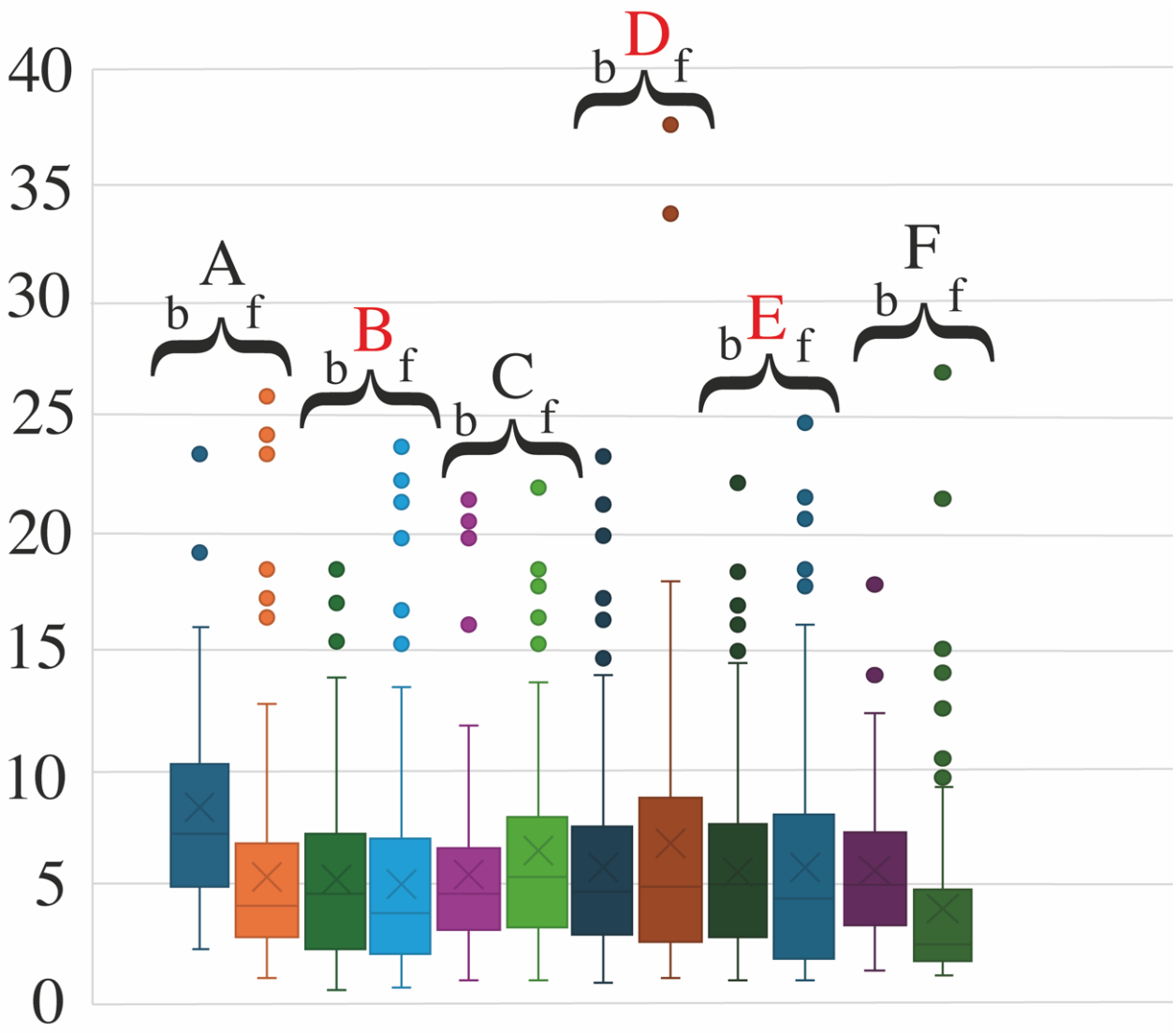

Figure 9. Box and whisker plots of maximum grain size measurements from *Difflugia* specimens A–F (B, D, E morphotype-A, and A, C, F morphotype-B), with b = rear half of test (towards fundus) and f = front half of test (towards aperture). Box and dot colour arbitrarily chosen.

Grains are not arranged on the test in a random fashion. In morphotype-B, and to a lesser extent morphotype-A, platey sheet-like micas and kaolin are preferentially placed around the fundus, while blockier or more granular feldspars, quartz and kaolin are arranged towards the aperture end (Figure 10). This is clearly illustrated in composite maps of Si and Al (Figure 11), where Si is a proxy for quartz and feldspars and Al for micas and kaolin. In addition, at least three samples clearly possessed smaller quartz grains, sometimes with feldspars, around their aperture (D7, D8, D10). In morphotype-A, tests can also be dominated by granular–blocky quartz and feldspar grains over the whole of the test, giving a rough texture (Figures 2B,E and 12). In both cases, longer grains are typically oriented parallel or sub-parallel to the long axis of the test (Figures 7D and 13, Table 3).

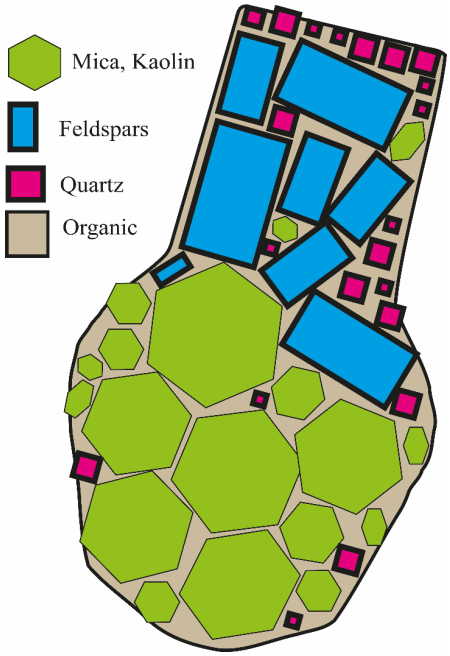

Figure 10. Schematic of *Difflugia*, illustrating relative preferred position of the three main mineral phases.

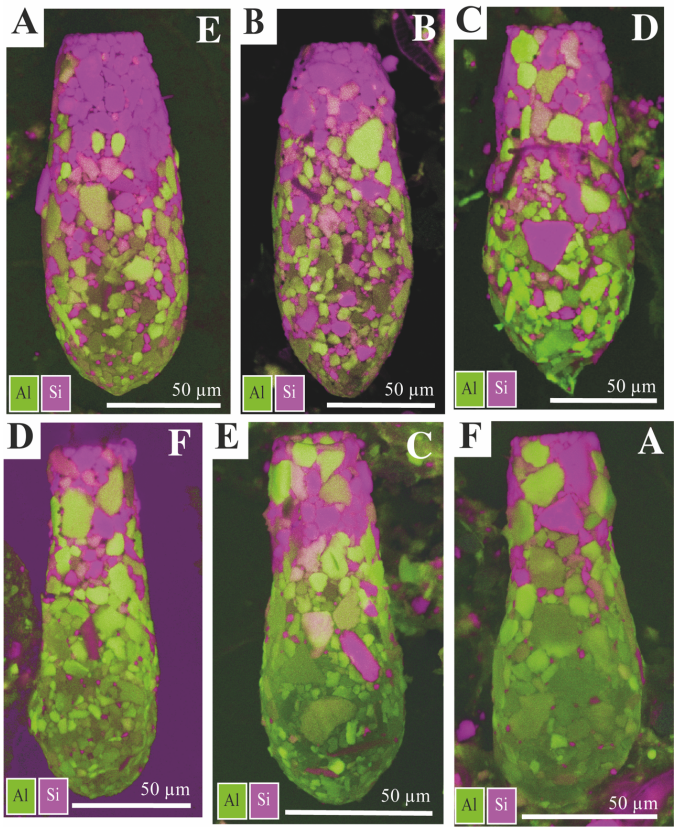

Figure 11. Si-Al elemental combined maps, to differentiate quartz rich areas (magenta) from alumino-silicate rich (feldspars, micas, kaolinite) areas (green). Note quartz illustrating a common preference for the apertural end of the test. (**A**–**C**) as in Figure 2A–C. (**D**–**F**) as in Figure 3A–C. White letters refer to specimen ID.

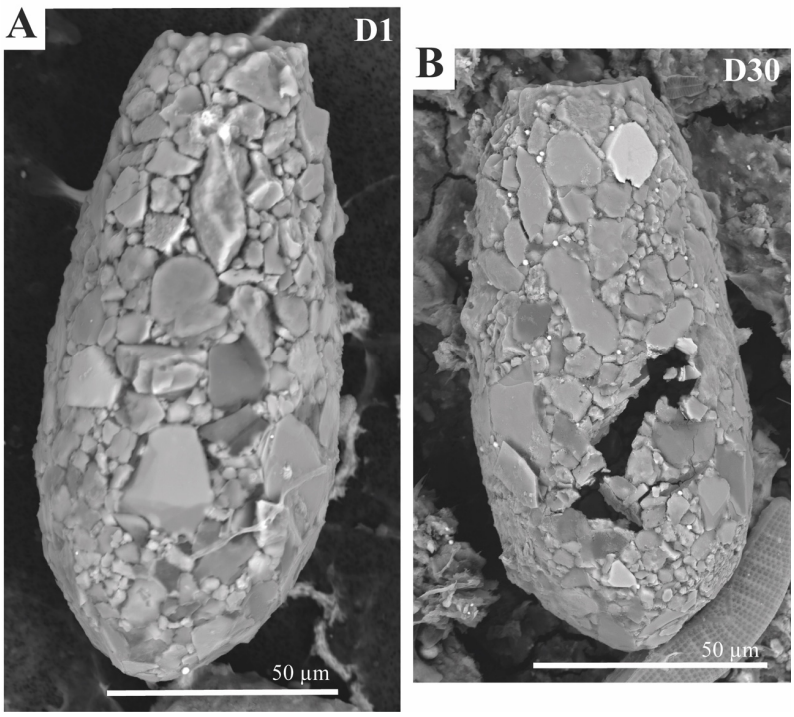

Figure 12. (**A**,**B**) BSE images of *Difflugia* sp. morphotype-A, where test is mainly covered in blocky or granular grains, dominated by framework silicates (feldspars and quartz). White letters refer to specimen ID.

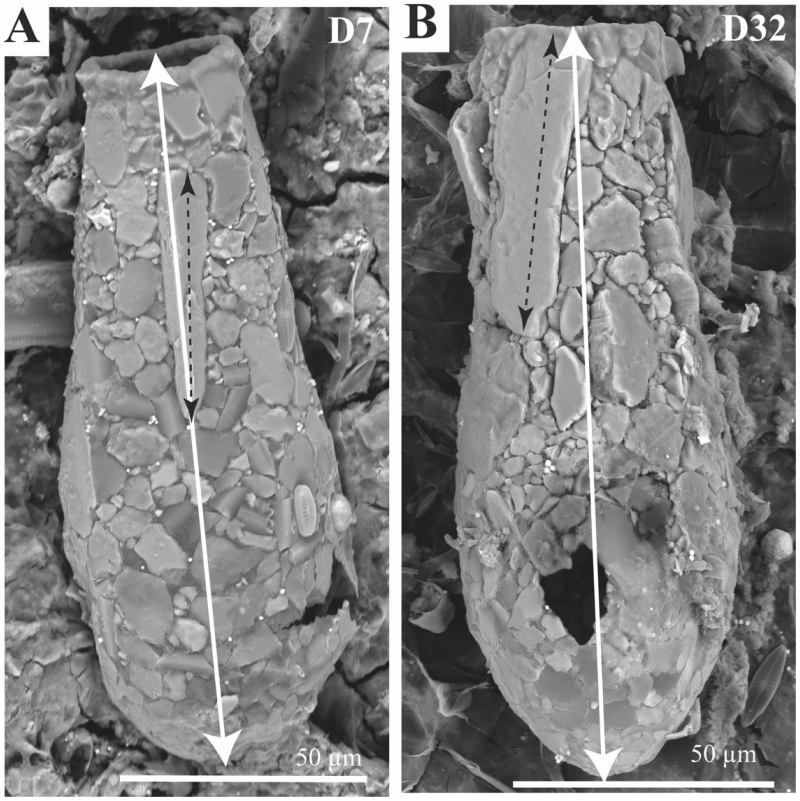

Figure 13. (**A**,**B**) BSE images of *Difflugia* sp. morphotype-B, illustrating the occurrence of elongated feldspar grains arranged parallel to test long axis. White double-headed arrow = long-axis of test, black double-headed dashed arrow = long-axis of feldspar grain. White letters refer to specimen ID.

4. Discussion

4.1. Taxonomic Identification

Due to the morphological variability known to occur within *Difflugia* species [5–8], their often polyphyletic nature and the occurrence of morphological convergence [8], the recent transfer of a number of *Difflugia* to *Cylindrifflugia* [8] and a lack of any molecular data for the current material, we here only identify the Gore Glen material as *Difflugia* sp., and as morphotype-A and -B. Morphotype-A has close affinity with *Cylindrifflugia lanceolata*, and *D. oblonga*, while morphotype-B's is with *Difflugia linearis*. Interestingly, Siemensma [4] illustrated a community of *Difflugia*, including lanceolate, pyriform, cylindrical and/or pointed forms, which, although containing *D. linearis*-like species *D. bryophila* and *D. lacustris*, exhibits no clear boundaries to reliably separate species. The samples examined herein represent a similar community, and although they are clearly separatable into two broad morphotypes, it is here deemed unwise to separate them at the species or potentially generic level (i.e., *Difflugia* spp., or *Difflugia* vs. *Cylindrifflugia*). It is also worth noting that *Difflugia pyriformis* from Leidy [9] incorporates both the above morphologies (see [6], Figure 6). The application of a more precise identification of the current material would unnecessarily complicate what in the case of *Difflugia*-like testate amoebae is already a frustrating conundrum. A total reassessment of the complex taxonomy of *Difflugia* and similar 'simple' xenosome-bearing flask shaped taxa (i.e., *Cylindrifflugia*) undoubtedly requires a long overdue in-depth analysis as recently illustrated by González-Miguéns et al. [8], in which more emphasis is placed on molecular phylogeny and less so on test grain composition, which can be controlled by sedimentological factors [2,3] or test shape. This would improve interpretation of the environmental significance of such taxa, while additional details on grain composition and size can be usefully utilised in other research areas such as testate amoebae interaction with the physical environment and questions over processes of grain selection.

4.2. Mineralogy

Châtelet et al. [2] used Raman microscopy and ESEM-EDS to successfully identify a range of minerals associated with the tests of agglutinated testate amoebae and associated sediments, through their elemental composition. Châtelet et al. [3] also used ESEM-EDS, with a range of mineral species being similarly identified, although noting that this was useless for distinguishing between orthoclase and plagioclase feldspars; the latter authors used microprobe analysis to differentiate albite, oligoclase and orthoclase. The current work using a combination of SEM-EDX with the addition of a BEX detector, here illustrates the success in using elemental colour overlay maps in differentiating quartz, feldspars, muscovite, kaolin and a range of other mineral phases, with supporting identification from AZtecMatch. Although not currently perfect, the use of AZtec Unity-BEX and AZtecMatch had a variable degree of success in terms of the degree of accuracy in identifying and separating mineral species. These are discussed below, along with other significant aspects of the mineralogy.

4.2.1. Quartz Versus Opal

Using the elemental colour scheme defined for the present work, both quartz and opal are magenta in colour. Quartz is typically assigned by AZtecMatch with a high degree of confidence (green). AZtecMatch shows some potential for differentiating opal and quartz, commonly suggesting either opal or quartz as the most likely identification (green), and at other times opal and quartz as equally a probable match (yellow). However, when morphology is taken into consideration (i.e., obviously biological opal such as diatoms and silicious cysts), the assignment of opal is seen not to be reliable. Herein, particles

AZtecMatch identified as either opal or quartz have been manually assigned as quartz. Apart from morphological differentiation, it was also noted that biogenic opal in some cases also contained carbon. This may prove worthy of further investigation for future developments using AZtecMatch.

4.2.2. Feldspars

The use of colour in the differentiation of feldspars using coloured composite AZtec BEX maps shows great potential in the identification of K-feldspar [blue] and Na-feldspars (albite) [purple]. Nevertheless, colour alone cannot 100% be used to predict the occurrence of the alkali feldspar anorthoclase, with a 50:50 occurrence of the latter occurring as either blue or purple, or in some cases colourless. For albite (plagioclase), 26 of 36 samples were directly assigned by AZtecMatch with confidence, with 10 at a lower level. Meanwhile, for orthoclase, only 7 out of 29 were assigned with the highest certainty, and 22 at a moderate level. Such problems may exist as both the alkali feldspars and plagioclases exist as solid-solution series [10]. In theory, this should make it easy to classify feldspars based on the constraints of the clearly defined fields of the orthoclase-albite-anorthite ternary diagram (see [10]). The current factory library is populated by 'standards' based on stoichiometric formulae. The acquisition of actual X-ray spectra, for specific feldspars, under the same collection parameters as used in imaging scans should help improve the precision for feldspar identification. Difficulties also exist in differentiating phases such as muscovite from alkali feldspars, as well as the potential issue of identifying weathered kaolinized feldspars.

4.2.3. Kaolin–Muscovite-Altered Muscovite/Feldspar

AZtecMatch identifies material as nacrite/dickite/halloysite/kaolinite. Given that these are all chemically $Al_2Si_2O_5(OH)_4$ and require X-ray diffraction (XRD) to correctly identify, we follow Gilkes and Prakongkep [11] in using 'kaolin' for such material. As far as we are aware, the occurrence of kaolin as grains used in test construction has not previously been reported for testate amoebae. The consistent identification of kaolin (nacrite/dickite/halloysite/kaolinite) by AZtecMatch is problematic. Typical kaolinite elemental spectra have approximately equal-sized peaks of Si and Al (see [12]). However, the kaolin clays can be more varied, with minor content of other ions (Ti, Mg, Na, K, Ca and Fe) [13], which can and here does cause tentative assignment to muscovite and a variety of feldspars. An additional complicating factor includes the known occurrence of kaolin minerals due to hydrothermal and diagenetic transformation of both muscovite and K-feldspar [14,15]. The latter is strongly suggested for some samples with a blocky feldspathic morphology, containing up to 12 atomic% K (average 5) and other ions such as Ca from 0–4 atomic% (average 1), Na 0–2 atomic% (average 0), and occasionally Fe. Therefore, material that has a green colouration in the coloured overlay maps may represent kaolin, muscovite or variably kaolinized mica or feldspars. Blockier material represents more 'massive' kaolin or perhaps kaolinized feldspar, while thinner platey examples are either single plates of kaolin or muscovite.

4.2.4. Pyrite

The occurrence of pyrite is easily detected from its bright yellow colouration in the layered elemental maps, its shape, small size (1 to 2 μm) and the presence of major peaks for iron and sulphur from both the X-Max and BEX systems. However, AZtecMatch did not conclusively identify pyrite, necessitating manual correction. This is likely due to the small size of the particles, with X-ray data being overwhelmed with signals from the surrounding silicate phases, and the small size of the beam interaction area solely within the pyrite (Figure 14). With the exception of Krivtsov et al. [1], noted in this area, this appears to

be the first time that single pyrite crystals have been recorded as actively selected by test building testate amoebae and purposefully placed. Other authors have only recorded pyrite as rare, and less than 1%, noting the occurrence of pyrite framboids [2,3]. At Gore Glen, pyrite is actively collected and utilised, as it is clearly cemented within the organic framework of the test (Figure 6A,B) and does not represent a diagenetic phase that has grown on the surface of the test. These small pyrite crystals originate from growth within the tests of chrysophacean algae (Figure 6C,D) on which the testate amoebae may have fed. Small nanometric-scale 'pimples' on the surface of the pyrite crystals utilised in the testate ameoba tests (Figure 6B) could be construed as modification to the crystal surfaces caused during the ingestion process. However, the same texture is also observed on the surfaces of framboidal pyrite formed within the chrysophacean cysts (Figure 6D).

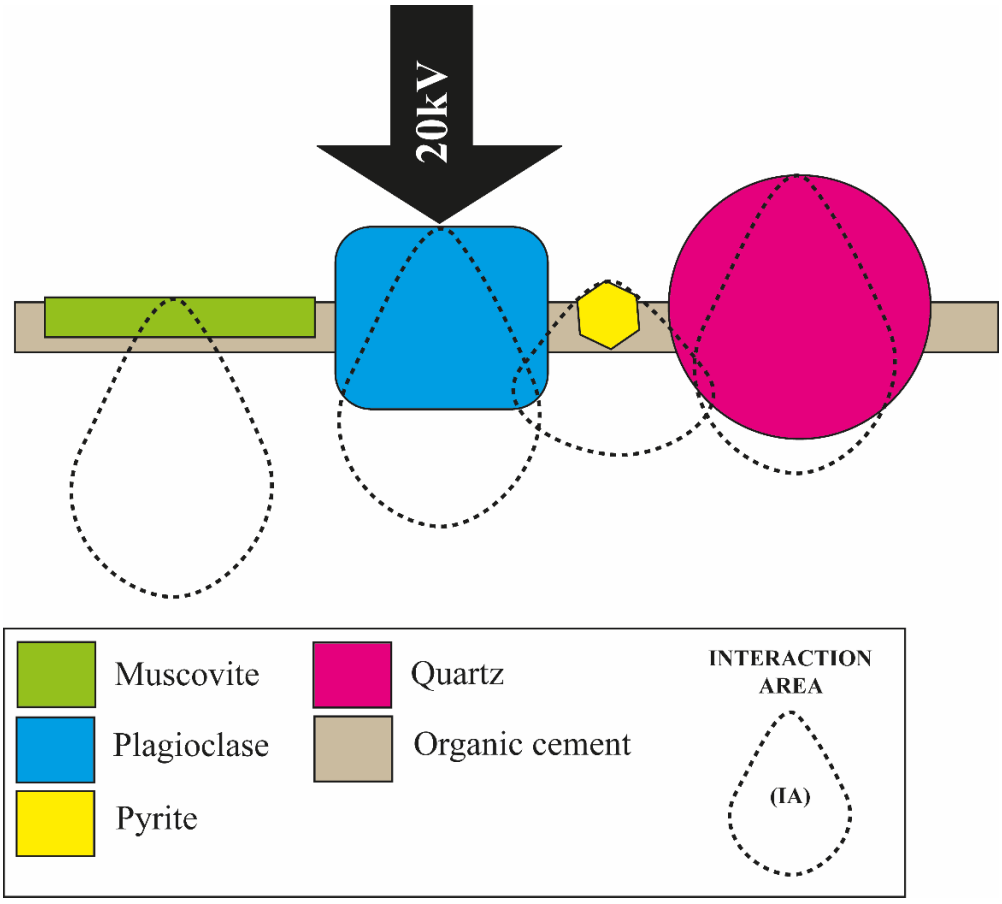

Figure 14. Schematic illustration of effect on elemental X-ray results due to beam penetration and interaction area (IA), with different mineral density, shape and size. Diagram represents cross-section through test.

4.2.5. Mg-Fe and Heavy Minerals

Garnet has not previously been recorded as a selected grain in either *Difflugia* or *Centropyxis* [2,3]. Nevertheless, garnet was offered as a suggestion in AZtecMatch on multiple occasions, although rarely with any great confidence. Further work collecting the spectra from a range of garnets will be required to improve this diagnosis. Grains identified as garnet by AZtecMatch may in part represent other Fe containing phases such as epidote, which has previously been noted within *Difflugia* [3].

Some particles could be interpreted as apatite, although the AZtecMatch software only gave apatite as a low-confidence choice, with identification being manually interpreted herein due to high Ca and P peaks in their spectra. Difficulty in identifying apatite appears to be due to the inclusion of Si and Al from surrounding grains (see Figure 14, example

for pyrite). Other heavy minerals observed included zircon and rutile. Zircon has not previously been identified by other authors, although rutile has previously been observed by Châtelet et al. [2] in *Centropyxis* and Châtelet et al. [3] recorded both Fe- and Ti-oxides from *Difflugia*.

Other Mg-Fe minerals such as hornblende, augite and biotite, based on composite maps, appear to be relatively rare but were not consistently positively identified in AZtex-Match, although amphibole has been noted in *Difflugia* by Châtelet et al. [3]. Lack of positive identification was in part due to the grains' small size or thinness (see Figure 14), as well as the requirement for a more representative AZtecMatch library for their identification.

4.2.6. Calcite

Calcite has previously been recorded as detrital particles from *Difflugia* and *Centropyxis* by other authors [2]. However, calcite recorded from the current material is rare and morphologically appears to represent precipitate within the pond, which has been selected for incorporation within the test. Calcite occasionally occurs within the pond, where it can form up to 25% of the total sediment load (Krivtsov unpublished data).

The current factory library only identifies calcite/aragonite. Although aragonite and calcite are stochiometrically identical, being polymorphs [16], biogenic aragonite has previously been differentiated by the presence of Sr within aragonite [17]. Further additions to the library, with such material, and other calcite-bearing Mg may help broaden the classification of $CaCO_3$ particles.

4.2.7. Biofilm Patches

Some areas, coloured green, magenta and yellow in the combined elemental maps (Supplementary Material D17, D21, D33), illustrate cracked surfaces (Figure 7B,E). These likely represent areas covered in patches of biofilm, with the colour coming from underlying feldspar/mica, quartz or iron-bearing minerals, respectively. These would normally be lost before imaging during standard preparation techniques utilised in testate amoebae studies, such as sample boiling to remove organic detritus and clean sample surfaces. The Fe-Mn cone-like structures and strings (Figure 7E,F), interpreted as biofilm structures, are interesting but not considered further herein as it is plausible that both forms of biofilm represent post-mortem alteration and degradation of the tests.

4.3. Comparison with Previous Work

4.3.1. Grain Size

Test grain size from Châtelet et al. [2] has a median value of under 5 µm, with most grain outliers less than 20 µm, compared to larger sediment modal values of between 56 and 88 µm. The associated sediments in Châtelet et al. [3] had a modal value of 151 µm, with a corresponding test grain size values being substantially smaller, with a maximum smaller than the aperture size of 70 µm [3] [test grain size given in volume rather than largest long axis]. The 1967 test grains measured during the current study generally agree with previous authors, commonly ranging from 2 to 10 µm, with a mean and average centred around 5 µm (Figure 9). However, in terms of the larger outlier grains the current material is larger than Châtelet et al. [2], but slightly smaller than that of Châtelet et al. [3]. As noted, Châtelet et al. [3] stated a maximum recorded test grain size of 70 µm. Given that the *Difflugia* in Châtelet et al. [3] is up to three times the size of the current material, this would suggest that maximum grain size is not dependent on test size, but rather, as stated by Châtelet et al. [3], is limited by the size of the aperture. In the current case, a number of particles are a lot larger than their aperture (Figure 13, Table 3). Nevertheless, in such cases, the grains are often elongated, and the minor grain axes are typically smaller than the aperture. Some larger grains are more equant in shape and have slightly larger dimensions

than their corresponding aperture (Table 3). The latter indicate that in the case of more equant-shaped grains, aperture size is the controlling factor limiting grain size utilised in test construction, but that it is the parent test aperture size, which may be slightly larger than that observed in the daughter test, that has the ultimate say. In the case of elongated grains, total grain length can be nearly twice the size of the aperture, and where used, these are typically positioned roughly parallel to the test's long axis (Figure 13, Table 3).

Histogram plots of all six selected individuals show a skewed distribution towards coarser grain sizes (Figure 8). However, maximum grain size is always under 40 µm, and therefore clay or silt-sized, with typically under 10 counts per specimen of 2 µm or less. Although such particles are clay-sized, they are not composed of clay minerals, but instead are pyrite- or clay-sized particles of quartz and feldspar. As with previous studies, grain selection for test formation at Gore Glen was selective towards the smaller end of the available sediment load, with only 10% of source sediment less than or equal to 45 µm (Krivtsov unpublished data).

The number of counted particles per specimen ranges between 208 and 382 per image, which equates to approximately 416 to 764 per test. This is less than that observed by Châtelet et al. [3] of 514 and 1265 grains total from *Difflugia*, but more than what may be considered reasonable given that the two examples in Châtelet et al. [3] are up to 3 times longer than the described Scottish material herein. This indicates no clear relationship between number of grains used (grain size) and overall test size.

No clear pattern in size distribution was noted between the back and front halves of the same individuals, or between the two identified morphotypes, with all plots overlapping in their distribution ranges (Figure 9).

4.3.2. Grain Composition

Châtelet et al. [2] used SEM-EDX analysis of thirty-two specimens of agglutinated testate amoebae (*Centropyxis* and *Difflugia*). They found that the *Centropyxis* samples from one locality were dominated by calcite (~70%–80%), with quartz, and ~8% feldspar. While at two other localities, *Centropyxis* were composed of quartz and mica (sericite), with some minor Fe oxide. A similar occurrence was also noted for the *Difflugia* within their study, with either a dominance of calcite grains, or both quartz and mica (Figure 15). No feldspar was noted in any of their *Difflugia*, although only one specimen had feldspar recorded from its corresponding sediment.

Châtelet et al. [3] examined the composition of two specimens of *D. oblonga* and found that the dominant grain type was quartz, followed by up to about 12% feldspar (Figure 15). No calcite was recorded despite its common occurrence within the contemporary associated sediment.

In the current work, samples are dominated by three major minerals, namely quartz, feldspars and mica/kaolin, with an approximately 50:50 ratio between quartz versus mica (including kaolin). Notably, morphotype-A tends to comprise more quartz than 'mica', and morphotype-B more 'mica' than quartz, although exhibiting a slight overlap. Despite calcite representing up to 25% of the sediment grain composition at Gore Glen (Krivtsov unpublished data), this was not reflected in grain usage within the thirty-nine examined samples. The Gore Glen sediment is dominated by quartz (28%–43%), with 2%–9% feldspar (Krivtsov unpublished data), which is in broad agreement with the noted usage of minerals within the test at this locality. However, anomalously, no mica or kaolin have previously been recorded from Gore Glen in substantial quantities.

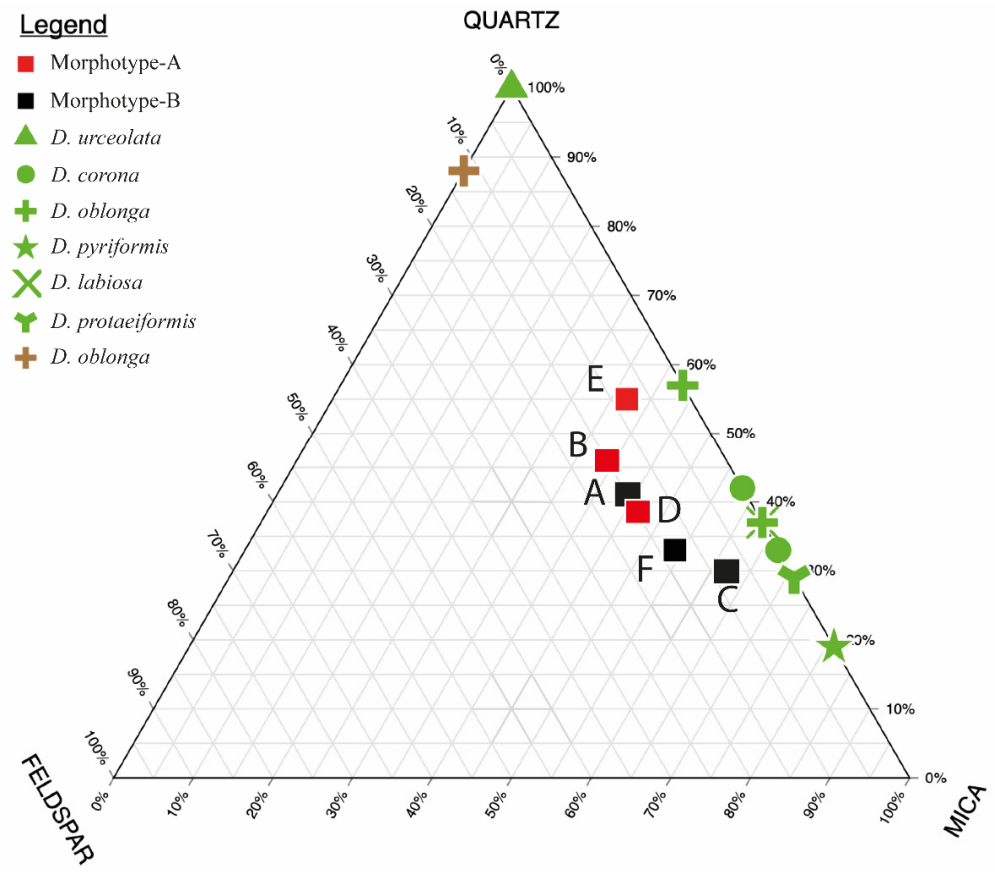

Figure 15. Ternary plot of detrital grain data for quartz, feldspar and mica used within '*Difflugia*'. Red and black squares from present study, samples A–F. Green plots = data from [2]), brown = [3]. Note that for the present study, mica also includes kaolin. Ratio of quartz to mica centred around 50:50 for the current study, with morphotype-A more quartz-rich and morphotype-B more mica-rich. Note data for Châtelet et al. [2] are more skewed in preference of mica (sericite). Feldspar content 8%–15% for current study. Made using TernaryPlot.com (accessed 28/9/24).

Therefore, although showing some similarities to previous studies, there is no close match in the details of the grain types utilised between the three studies (Figure 15). This is not surprising, as *D. oblonga* from both previous studies [2,3] did not correspond in their composition of grain types utilised, other than that both contained quartz. The Scottish material in terms of quartz, feldspar and mica has a broader spectrum of grain utilization, with a more multi-modal mineralogical usage profile compared to those of Châtelet et al. [2,3] which are dominated by the selection and usage of only one or two major grain types.

With the exception of small particles of quartz around the aperture [2,3], previous studies have not noted any major preferred grain placement based on mineralogical selection for particular areas of the test of *Difflugia*. In the current study, as noted, some specimens also display a preference for the placement of small granular quartz grains around the aperture (Figures 2E,F and 3D). However, for the current material using maps of elemental distribution for Si and Al as proxies for the framework silicates quartz and feldspar, versus the sheet silicates muscovite and kaolin (Figure 11), indicates that the former are commonly concentrated around the anterior end (apertural half), while the latter occur more dominantly around the posterior end (towards the fundus). This is also supported from examination of BSE and composite elemental overlay maps (Figures 2 and 3, File S1 in Supplementary Material). In addition, pyrite in some cases preferentially occurs within the anterior portion of the test, towards the aperture, where

it is found filling in between larger grains within the organic cement (Figure 6A,B). This appears to be the first time that an ordered variation in the placement of mineral grain types, using elemental X-ray mapping, has been noted for *Difflugia*. Other mineral phases show no apparent preference in their positioning within the test.

4.4. Purpose of Grain Selection and Preferred Distribution

It has previously been suggested that testate ameobae such as *Difflugia* select for grains that have a similar specific gravity to maintain neutral buoyancy [3]. We would not dispute this possibility; however, the current material does not necessarily support the theory, as specific gravity varies greatly (Table 5), with quartz, feldspar, muscovite and kaolinite (2.16–3.00) to pyrite and heavy minerals (4.6–5.10). In fact, the occurrence in some cases of pyrite concentrated towards the apertural end of the test and the preferred distribution of more bulky grains towards the aperture and thinner (less volumetric) sheet-silicates around the rear portion of the test suggests the possibility that in some cases, variation in grain density could help in keeping the aperture orientated in a downwardly inclined direction (Figure 16). However, as water has a specific gravity of 1.00, it is uncertain as to how much of an effect such variation in specific gravity across the test of *Difflugia* would have in relationship to the attitude of such tests.

Table 5. Specific gravity of main identified mineral phases (data from [13]).

Mineral	Specific Gravity
Quartz	2.59–2.63
Feldspar	2.55–2.76
Muscovite	2.76–3.00
Kaolinite	2.16–2.68
Apatite	3.16–3.22
Ilmenite	4.70–4.79
Zircon	4.60–4.70
Pyrite	4.95–5.10
Rutile	4.23
Garnet	3.1–4.3
Hornblende	2.9
Biotite	2.7–3.3

As well as specific gravity, the common minerals observed in the current tests of *Difflugia* possess a range of wettability conditions. Most are hydrophilic (water wet), such as quartz, feldspar and mica [18–20]. Pyrite is known to be superhydrophilic [21]. Kaolinite (001) faces are hydrophilic, with other faces hydrophobic [18], and weathered feldspars can be oil wet (hydrophobic) due to the formation of clays [18]. No immediately obvious advantage to selecting grains with different wettability characteristics comes to mind. It may be possible that the superhydrophilic nature of pyrite could have helped retain a film of water across the apertural end of the test in environmental settings where the testate amoebae are temporally exposed to air. However, no evidence of this occurring was noted at the current location.

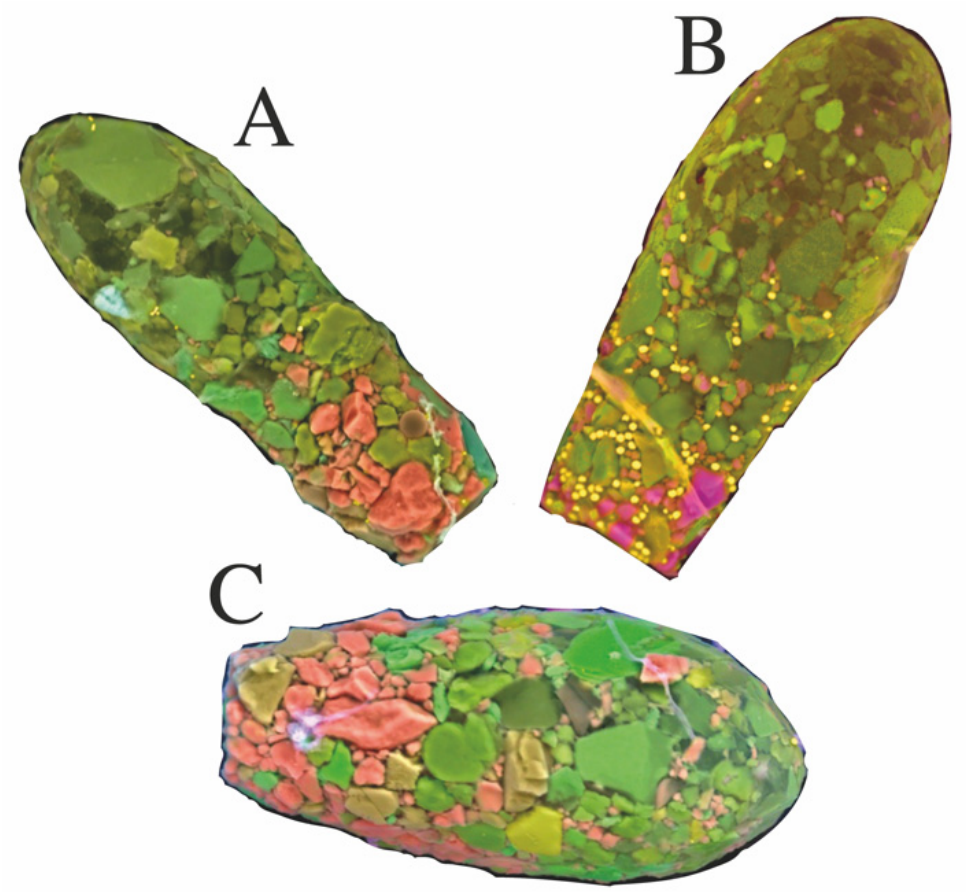

Figure 16. Potential test life orientation, based on mineral distribution density differences. (**A**) Inclined, blocky denser minerals towards aperture, and lighter thinner minerals at fundus. (**B**) As in (**A**), with addition of denser pyrite crystals at the aperture-end. (**C**) Horizontally orientated test, with more evenly distributed similar density/blocky grains.

One alternative theory to explain the observed compositional variation, particularly observed in morphotype-B, is that this reflects different structural properties of the grain types, with grains being selected and distributed based on functional structural reasons. In such a case, blockier, more rigid grains of quartz and feldspar are utilised to form the more cylindrical front half of the test, while lighter, thinner, more flexible particles of mica and kaolin dominate around the rear half of the test, where they form an overlapping and interlocking jigsaw of components forming the more complex geodesic shape of this area, and additionally produce a smooth inner surface for the internal cellular components. Such a functional use would be similar to the interpretations of Dumack et al. [22], into the structural use of the test of Arcellinida as a weapon. It is of course also possible that the observed distribution of grain types reflects more than one controlling mechanism, possibly in relationship to both structural parameters and specific gravity of the utilised components.

5. Conclusions

BEX, BSE/X-ray maps clearly illustrate the occurrence and distribution of multiple mineral species forming the tests of *Difflugia*. This should be equally applicable to other xenosome-bearing testate amoebae such as *Centropyxis* and *Cyclopyxis*.

AZtecMatch is useful for identifying the mineral phases present but requires further work on mineral libraries for some of the commonly occurring minerals associated with testate amoebae tests.

In the context of the current work, automated grain analysis is problematic exasperated where grains are thin (i.e., micas and platey clays) or where particles are smaller than the beam penetration depth (i.e., particularly pyrite and heavy minerals such as apatite).

The occurrence of heavy mineral phases, and particularly the positioning of pyrite towards the aperture end of the test, may result in alteration to the buoyancy of tests and their orientation in respect to the environment.

The reported occurrence of clay particles (kaolin) is reported here for the first time. The significance of its use is as yet uncertain.

Particle size distribution across the test generally show no strong preferential distribution. One exception to this being the occurrence of small more granular quartz and feldspar grains as a ring around the aperture of some tests.

In the current examples there is a preference for sheet-silicates (micas and kaolin) towards the fundus, and framework silicates (quartz and feldspar) towards the aperture (Figures 2, 3, 10 and 11). We postulate that this is based upon mineral structural properties, rather than mineralogy *per se*. Thin (platey) flexible mineral phases are placed around the fundus, while stronger more robust framework silicates (quartz, feldspars) are preferentially placed at the anterior portion of the test.

Primary control on grain size and mineralogy is controlled by local sediment availability [2,3]. Selection and placement from the available sediment pool may be based on structural considerations–in this case sheet-silicates versus framework silicates. We therefore suggest that the use of parameters such as xenosome size, size distribution, composition and distribution and even overall test shape should be used carefully in taxonomic works, as many appear to be of limited taxonomic significance.

Supplementary Materials: The following supporting information can be downloaded at: https://www.mdpi.com/article/10.3390/min15010001/s1, BSE images, colour overlay elemental maps and individual elemental maps for all specimens examined during the present work (thirty-nine) are included in the Supplementary Material section (File S1). In addition, elemental X-ray data obtained through EDX analysis are available in File S2.

Author Contributions: Conceptualization, J.B.; methodology, J.B.; formal analysis, J.B. and V.K.; investigation, J.B. and V.K.; resources, J.B.; data curation, J.B. and V.K.; writing—original draft preparation, J.B. and V.K.; writing—review and editing, J.B. and V.K.; visualization, J.B. All authors have read and agreed to the published version of the manuscript.

Funding: This research received no external funding.

Data Availability Statement: All available data are contained within the Supplementary Material.

Acknowledgments: We acknowledge the use of the scanning electron microscopy facility at the Institute of GeoEnergy Engineering, Heriot-Watt University.

Conflicts of Interest: The authors declare no conflict of interest.

References

1. Krivtsov, V.; Buckman, J.; Birkinshaw, S.; Olive, V. Interactions of hydrology, geochemistry, and biodiversity in woodland ponds located in riverine floodplains: Case study from Scotland. *Environ. Sci. Pollut. Res.* **2023**, *31*, 40678–40693. [CrossRef] [PubMed]
2. du Châtelet, E.A.; Guillot, F.; Recourt, P.; Ventalon, S.; Tribovillard, N. Influence of sediment grain size and mineralogy on testate amoebae test construction. *Comptes Rendus Geosci.* **2010**, *342*, 710–717. [CrossRef]
3. du Châtelet, E.A.; Noiriel, C.; Delaine, M. Three-Dimensional Morphological and Mineralogical Characterization of Testate Amebae. *Microsc. Microanal.* **2013**, *19*, 1511–1522. [CrossRef] [PubMed]
4. Siemensma, F.J. *Microworld, World of Amoeboid Organisms*; World-Wide Electronic Publication: Kortenhoef, The Netherlands, 2024.
5. Mazei, Y.; Warren, A. A survey of the testate amoeba genus Difflugia Leclerc, 1815 based on specimens in the E. Penard and C.G. Ogden collections of the Natural History Museum, London. Part 1: Species with shells that are pointed aborally and/or have aboral protruberances. *Protistology* **2012**, *7*, 121–171.

6. Mazei, Y.; Warren, A. A survey of the testate amoeba genus Difflugia Leclerc, 1815 based on specimens in the E. Penard and C.G. Ogden collections of the Natural History Museum, London. Part 2: Species with shells that are pyriform or elongate. *Protistology* **2014**, *8*, 133–171.
7. Mazei, Y.; Warren, A. A survey of the testate amoeba genus Difflugia Leclerc, 1815 based on specimens in the E. Penard and C.G. Ogden collections of the Natural History Museum, London. Part 3: Species with shells that are spherical or ovoid. *Protistology* **2015**, *9*, 3–49.
8. González-Miguéns, R.; Todorov, M.; Blandenier, Q.; Duckert, C.; Porfirio-Sousa, A.L.; Ribeiro, G.M.; Ramos, D.; Lahr, D.J.G.; Buckley, D.; Lara, E. Deconstructing *Difflugia*: The tangled evolution of lobose testate amoebae shells (*Amoebozoa: Arcellinida*) illustrates the importance of convergent evolution in protist phylogeny. *Mol. Phylogenet. Evol.* **2022**, *175*, 107557. [CrossRef] [PubMed]
9. Leidy, J. Fresh-water rhizopods of North America. In *Report of the United States Geological Survey of the Territories*; Government Printing Office: Washington, DC, USA, 1879; Volume 12, pp. 1–324. [CrossRef]
10. Scheibe, C. The Feldspar Compositional Ternary Diagram. 2021. Available online: https://chemostratigraphy.com/feldspar-compositional-ternary-diagram/ (accessed on 7 November 2024).
11. Gilkes, R.J.; Prakongkep, N. How the unique properties of soil kaolin affect the fertility of tropical soils. *Appl. Clay Sci.* **2016**, *131*, 100–106. [CrossRef]
12. Welton, J.E. *SEM Petrology Atlas*; Methods in Exploration Series; The American Association of Petroleum Geologists: Tulsa, OK, USA, 1984.
13. Wikipedia contributors. Wikipedia, The Free Encyclpedia. 2024. Available online: https://en.wikipedia.org (accessed on 7 November 2024).
14. Marfil, R.; Delgado, A.; Rossi, C.; La Iglesia, A.; Ramseyer, K. Origin and diagenetic evolution of kaolin in reservoir sandstones and associated shales of the Jurassic and Cretaceous Salam Field, Western Desert (Egypt). In *Clay Mineral Cements in Sandstones*; Worden, R.H., Morad, S., Eds.; Wiley: Hoboken, NJ, USA, 1999. [CrossRef]
15. Yuan, J.; Yang, J.; Ma, H.; Su, S.; Chang, Q.; Komarneni, S. Hydrothermal synthesis of nano-kaolinite from K-feldspar. *Ceram. Int.* **2018**, *44*, 15611–15617. [CrossRef]
16. Janiszewska, K.; Mazur, M.; Machalski, M.; Stolarski, J. From pristine aragonite to blocky calcite: Exceptional preservation and diagenesis of cephalopod nacre in porous Cretaceous limestones. *PLoS ONE* **2018**, *13*, e0208598. [CrossRef] [PubMed]
17. Buckman, J.O.; Harries, D.B. Reef forming *Serpula vermicularis* from Scotland and Ireland: Tube structure, composition and implications. *Zool. Anz.* **2020**, *288*, 53–65. [CrossRef]
18. Barclay, S.A.; Worden, R.H. Effects of reservoir wettability on quartz cementation in oil fields. *Spec. Publ. Int. Assoc. Sedimentol.* **2000**, *29*, 103–117.
19. Szczes, A.; Chibowski, E.; Rzeznik, E. Magnetic field effect on water surface tension in aspect of glass and mica wettability. *Colloids Interfaces* **2020**, *4*, 37. [CrossRef]
20. Buckman, J.O. ESEM Application Note: Wettability studies of petroleum reservoir rocks. FEI technical note. *ESEM Appl. Note* **2000**, *10*. [CrossRef]
21. Rahman, M.Z.; Thyr, J.; Edvinsson, T. Surface polarity, water adhesion and wettability behaviours of iron pyrite. *Mater. Today Proc.* **2020**, *33*, 2465–2469. [CrossRef]
22. Dumack, K.; Lara, E.; Duckert, C.; Ermolaeva, E.; Siemensma, F.; Singer, D.; Krashevsha, V.; Lamentowicz, M.; Mitchell, E.A.D. It's time to consider the *Arcellinida* shell as a weapon. *Eur. J. Protistol.* **2024**, *92*, 126051. [CrossRef]